Electronic Supplementary Material (ESI) for Chemical Communications

Supporting Information

Halogen Bonds as Stabilizing Interactions in a Chiral Self-Assembled Molecular Monolayer

Rico Gutzler,*[a,b] Oleksandr Ivasenko,[a] Chaoying Fu,[a,b] Jaclyn L. Brusso,[a,§] Federico Rosei,*[,b] and Dmitrii F. Perepichka*[,a]

[a] *Department of Chemistry and Centre for Self-Assembled Chemical Structures, McGill University, 801 Sherbrooke Str West, Montreal, QC, H3A 2K6, Canada; E-mail: dmitrii.perepichka@mcgill.ca*
[b] *Institut National de la Recherche Scientifique and Centre for Self-Assembled Chemical Structures, Université du Québec, 1650 boulevard Lionel-Boulet, Varennes, QC, J3X 1S2, Canada; E-mail: rosei@emt.inrs.ca; gutzler@emt.inrs.ca*
[§] *Present address: Department of Chemistry, University of Ottawa*

Contents

Electronic Supplementary Material (ESI) for Chemical Communications

I. Methods

STM

A drop of saturated solution of 2,5,9,12-tetrabromotrithieno[2',3':5,6:3',2':3,4:3',2':7,8]anthra[1,2-b]thiophene (TBTTA) in 1,2,4-trichlorobenzene was applied to a freshly cleaved graphite(001) surface. STM topographs were recorded with the tip immersed in solution in constant current mode with a Digital Instruments Inc. (Veeco) NanoScope IIIa STM at room temperature. Platinum-Iridium (80/20) tips were cut from a 0.25 mm wire. Volumes of 2-5 μL of solution were applied to the surface, all volumes yielding the same molecular monolayer. Lattice constants of the 2D molecular structure were determined from images in which both the graphite substrate and the supramolecular structure were imaged. Tunnelling bias is reported with respect to the tip. Single-molecule defects in the close-packed molecular structure were used to identify the orientation of the molecule within the unit cell (see Fig. S2).

DFT

DFT calculations were performed with Gaussian 09.[1] In order to account for weak van der Waals interactions, the M06-L and M06-2X functionals were used, together with the 6-31G(d,p) basis set. The M06 functionals were shown to give improved results for weakly bonded systems compared with other functional.[2,3] For comparison, also the B3LYP functional was used with the same basis set. Calculations were done on isolated molecules, small clusters, and with periodic boundary conditions (PBC). Atom positions were fixed in the direction perpendicular to the molecular plane and allowed to relax only in-plane to approximate the influence of the neglected substrate. In the PBC calculations, the lattice vectors were not constrained. Binding energies within the 2D network are computed as single point calculations with the geometry taken from the PBC results. A large cell is constructed from four small single molecule cells and its energy is calculated. In the following step, the energy of one molecule in this cell is calculated, and subsequently the energy of the remaining three molecules. Binding energies are corrected for the basis set superposition error (BSSE) by calculating counterpoise corrected energies.[4,5] Natural bond orbitals were analyzed using Gaussian NBO Version 3.1 as implemented in Gaussian 09.[6]

Table SI: Additional close-contact distances for the M06-L and B3LYP functional (all with 6-31G(d,p) basis set).

	Sum of van-der-Waals Distances	Distance/Å (M06-L)	Distance/Å (M06-2X)	Distance/Å (B3LYP)[a]
D1 Br···Br	3.70	3.38	3.42	3.66
D2 Br···S	3.65	3.64	3.64	3.49
D3 Br···S	3.65	3.41	3.41	4.06
D4 Br···H	3.05	2.93	2.95	2.99
D5 Br···H	3.05	2.87	2.86	3.25
D6 S···S	3.60	3.52	3.50	3.85

[a] The unit cell optimized with the B3LYP functional measures a = 1.14 nm, b = 1.44 nm, α = 71°.

II. Additional STM Data

The moiré pattern in the TBTTA monolayer observed by STM (see Fig. S1) is possibly due to a periodic modulation of the interaction of single TBTTA molecules with the substrate. Different adsorption sites on the surface influence the electronic structure in such a way that the contrast in the STM topograph is altered. The matrix M that relates the single molecule unit cell vectors $\vec{a}, \vec{b}$ with the larger unit cell vectors $\vec{A}, \vec{B}$ that describes the moiré pattern (see Fig. 1b main text) is $M = \begin{pmatrix} 40 & -2 \\ -7 & 6 \end{pmatrix}$, with $\begin{pmatrix} \vec{A} \\ \vec{B} \end{pmatrix} = M \begin{pmatrix} \vec{a} \\ \vec{b} \end{pmatrix}$.

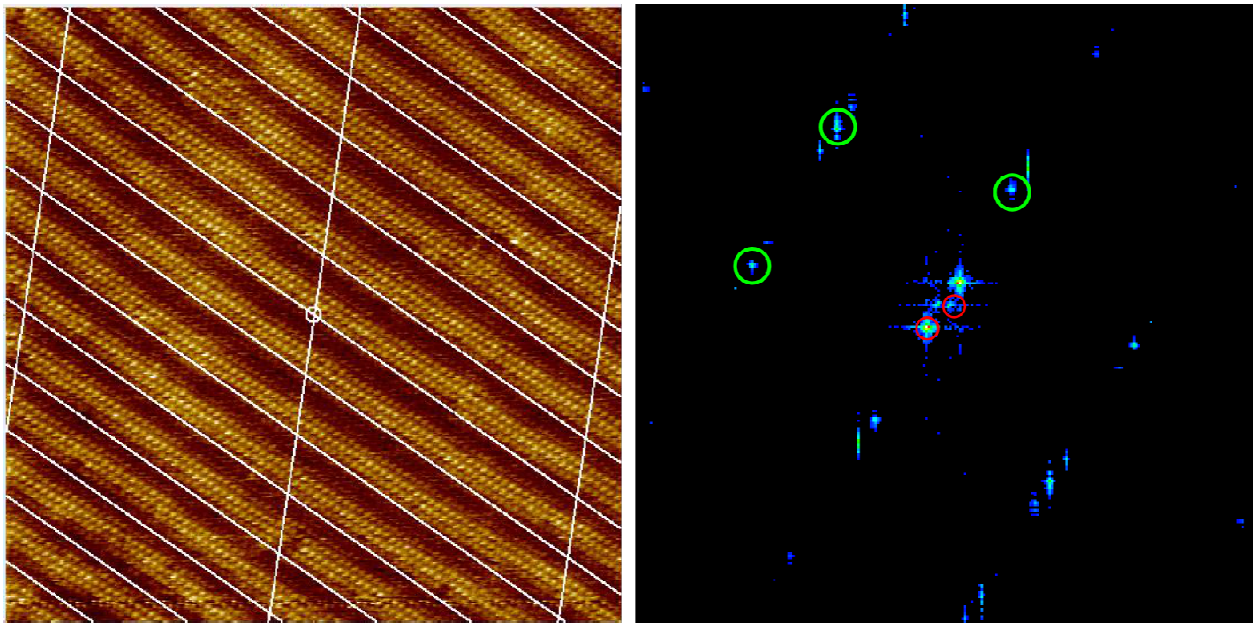

Figure S1. Same topograph as Fig. 1b in main text (left) with corresponding Fourier transform (right). The green circles indicate the reflexes of the single molecule unit cell, while the red circles indicate the reflexes that correspond to the moiré pattern. The periodic mesh that is defined by these reflexes is presented in the left topograph.

Defects, i.e. missing molecules, in the supramolecular structure decisively help to evaluate the adsorption geometry of molecules in the monolayer.

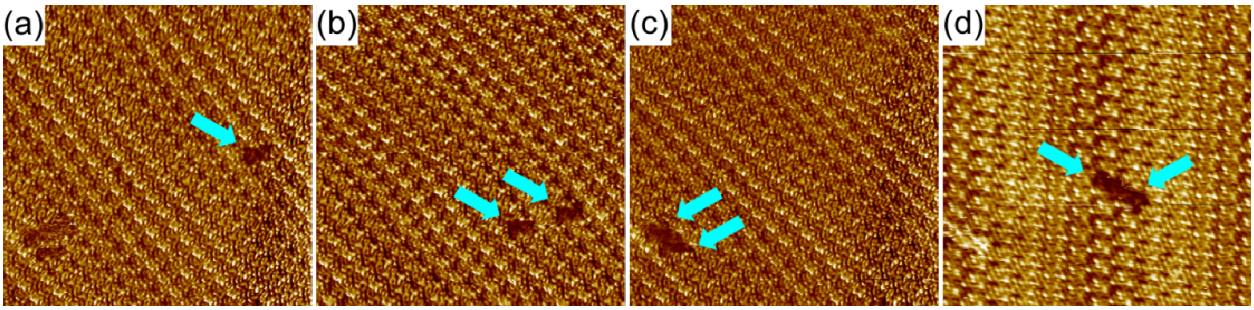

Figure S2. STM topographs with defects (indicated by blue arrows) in the molecular monolayer. All images 20 × 20 nm. (a) Single molecule defect. (I_T = 900 pA, V_{bias} = 500 mV) (b) Two single molecule defects separated by one unit cell. (I_T = 900 pA, V_{bias} = 500 mV) (c) Two adjacent missing molecules. This defect corresponds to two molecules in the long side binding configuration (*cf.* Fig. 2 main text). (I_T = 900 pA, V_{bias} = 500 mV) (d) Two adjacent missing molecules in the short side binding configuration. (I_T = 100 pA, V_{bias} = -800 mV)

The long side of the unit cell aligns with a high symmetry axis of the underlying graphite lattice, while the small side runs with a ~10° angle with respect to the next axis.

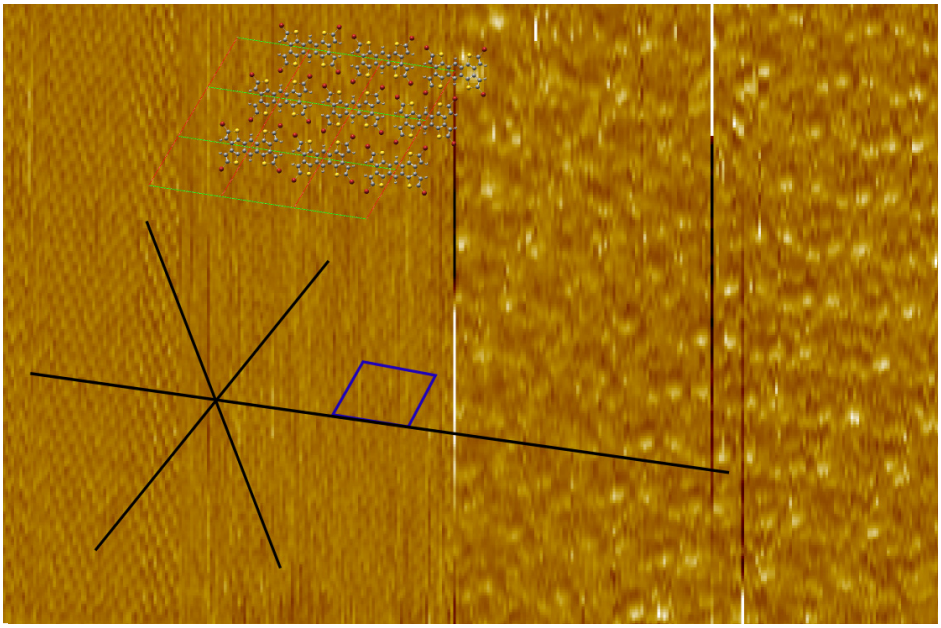

Figure S3. Topograph of the graphite surface (left) and molecular suprastructure (right). The high-symmetry axes of the graphite are indicated in black. The blue cell is constructed from

periodic features in the right part of the image. In the upper part of the topograph, the output of the 2D DFT calculation is overlaid scaled to size.

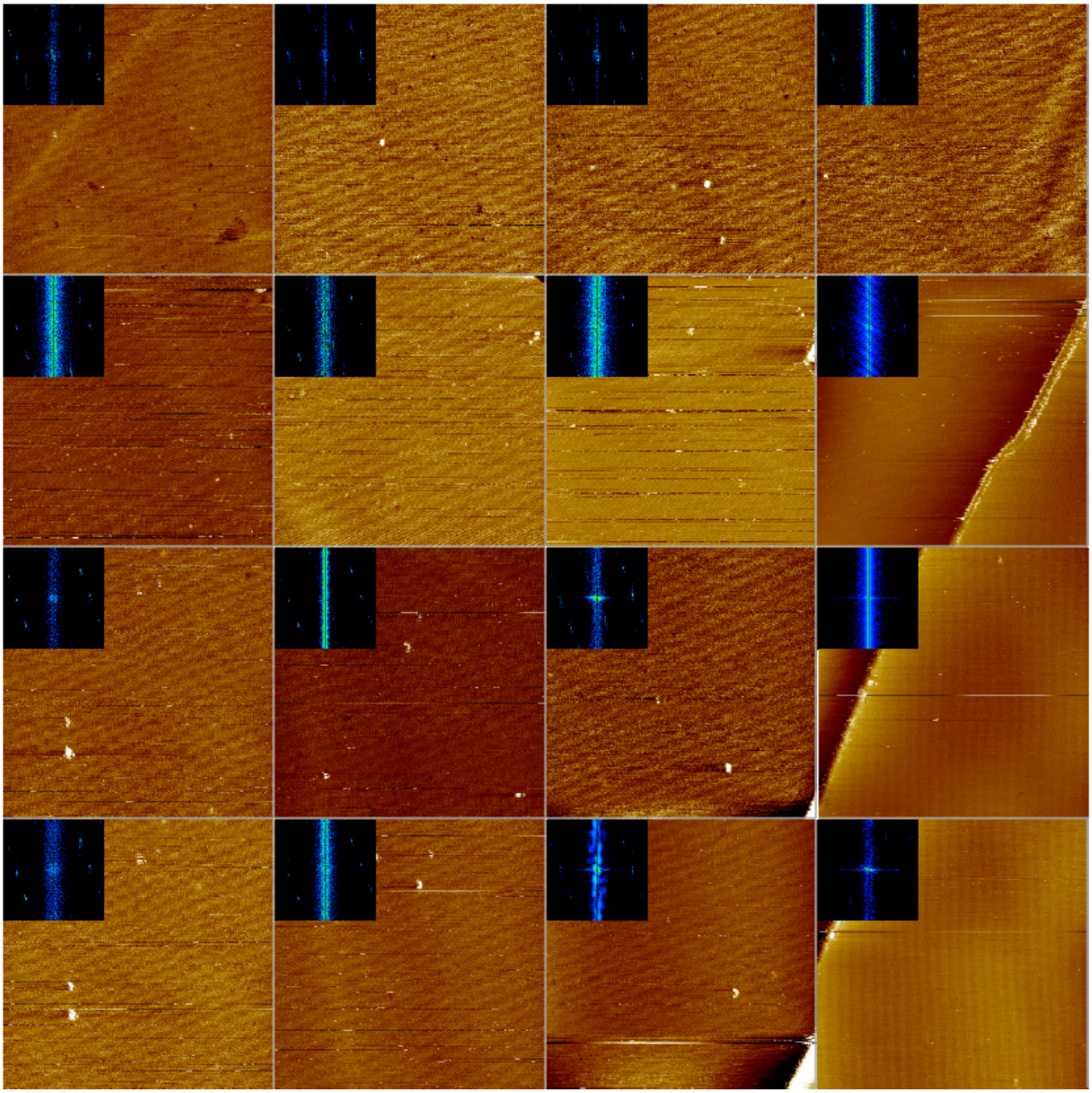

Figure S4. Grid of 4 × 4 200 nm topographs. The striped moiré pattern is discernible running diagonal from upper right to lower left in each image. The imaged area of 640000 nm^2 is covered by one single domain of TBTTA molecules, except for the terrace to the lower right, where a domain with different orientation is observed. Spots corresponding to the periodic single molecule unit cell are shown in the Fourier transforms of each topograph. (all images I_T = 300 pA, V_{bias} = 800 mV)

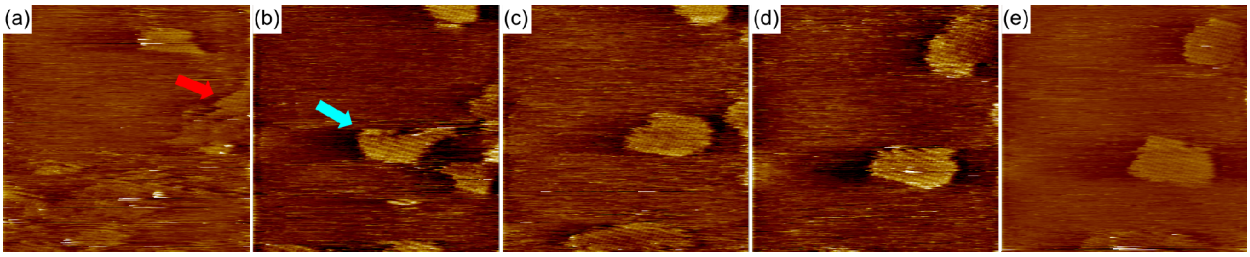

Figure S5. STM topographs after annealing the sample to 60 °C until the solvent is evaporated (all images acquired at room temperature, 80 nm × 80 nm, 16 seconds time laps in between two consecutive topographs). No stable monolayer was observed, only small unstable patches. The red arrow points at a domain at the right border which disappears over time. The blue arrow points at a domain that assembles quickly from (a) to (b). Its shape is fluctuating with time due to molecule attachment and detachment from the island. (all images I_T = 150 pA, V_{bias} = 1200 mV)

In the submonolayer regime and without the solution as reservoir of additional TBTTA molecules, the self-assembled domains on the graphite surface are not stable. Dynamic processes, attachment and detachment of freely diffusing molecules, can be observed. This quick dynamics has its origin in the low binding energy of one TBTTA molecule in the monolayer. The same process is responsible for fast Ostwald ripening which eventually leads to the formation of large domains.

III. Additional DFT Data

The asymmetry in the electrostatic potential of TBTTA observed for the molecule in the supramolecular structure as compared to the isolated molecule is also reflected in an asymmetry in the molecular orbitals (Figure S6). The occupied and unoccupied orbitals of the undisturbed molecule (upper row) are more regular than those of TBTTA in the 2D network (lower row). This effect is larger for the occupied orbitals than for the unoccupied orbitals.

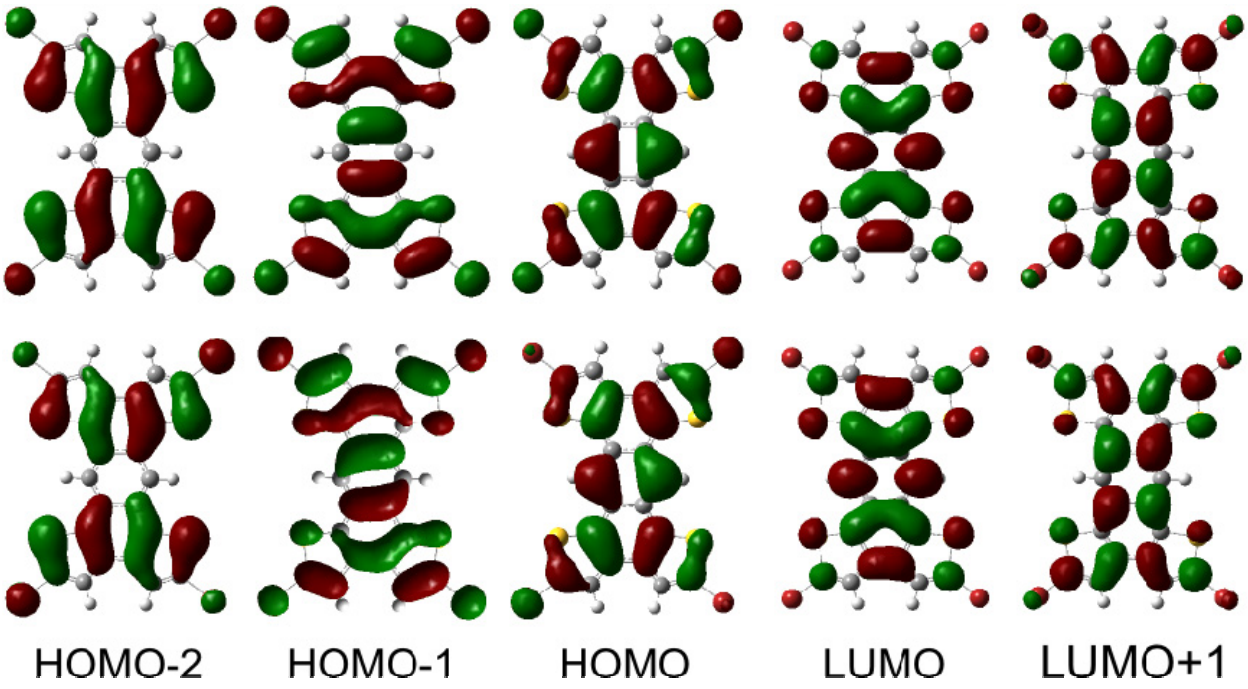

Figure S6. Molecular orbitals from the M06-2X calculations. Upper row: Orbitals from isolated molecule. Lower row: Orbitals for molecule in 2D network. Small changes between undisturbed molecule and molecule in supramolecular structure can be discerned, also manifested in a reduced symmetry of the latter. These changes are more dominant in the occupied orbitals than in the unoccupied orbitals.

Additional Structures

In addition to the experimentally observed structure (Fig. S7), two further polymorphs have been calculated with the M06-2X functional. The experimentally observed structure in the PBC calculation yields a binding energy of -3.1 kcal mol^{-1}. 12 contacts per molecule between heavy atoms can be identified.

The first alternative structure corresponds to a symmetric, achiral structure (Figure S8) with a binding energy of -1.1 kcal mol^{-1}. The lattice vectors are a = 1.35 nm, b = 1.37 nm, α = 71°. This polymorph is less stable albeit the larger number of possible contacts between heavy atoms (16).

The third structure (Figure S9), which like the observed structure is chiral, is found to be energetically slightly more stable (-3.2 kcal mol^{-1}, a = 1.13 nm, b = 1.42 nm, α = 95°). The only stabilizing contributions are from a rectangular arrangement of Br atoms that allow for close to optimal Br···Br interaction. Although the number of contacts between heavy atoms is the smallest (8), the optimal geometry for halogen···halogen bonds yields to the highest stabilization energy. Nevertheless, the larger unit cell compared to the experimentally observed polymorph renders this structure energetically less favorable. The energy per unit area accounts to 6.44 kcal m^{-2} in this structure versus 7.04 kcal m^{-2} in the experimental polymorph, without taking into account interactions with the substrate.

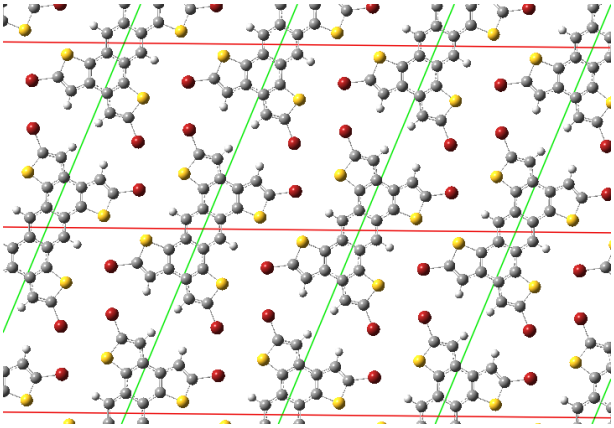

Figure S7. Optimized experimentally observed unit cell.

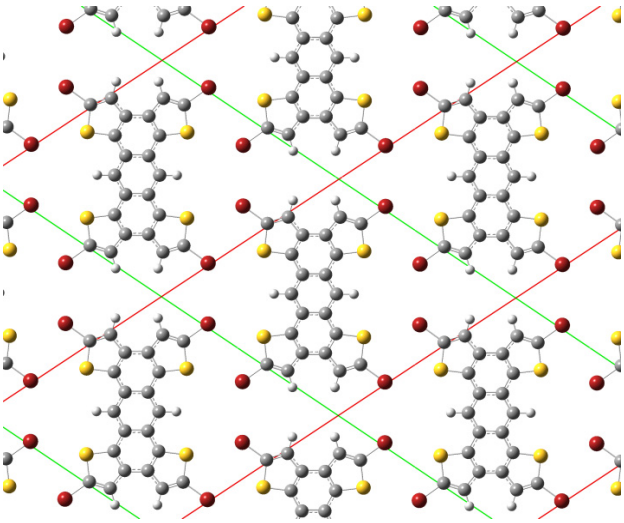

Figure S8. Achiral 2D structure.

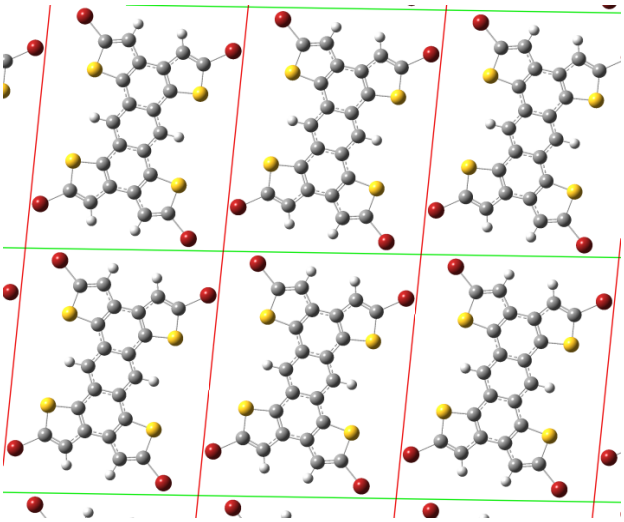

Figure S9. Alternative chiral 2D structure.

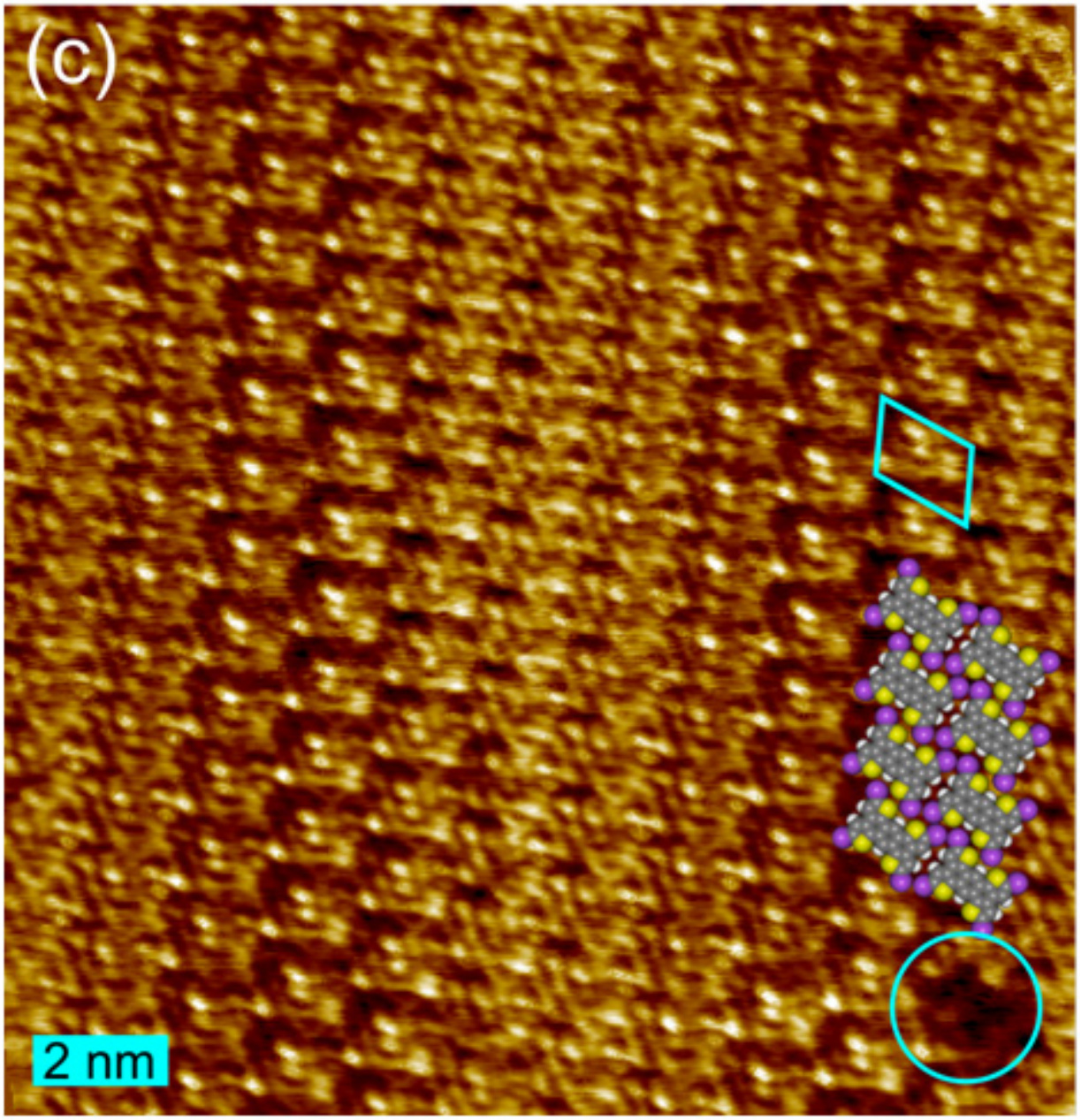

Figure S10. Larger-scale copies of the Fig. 1c.

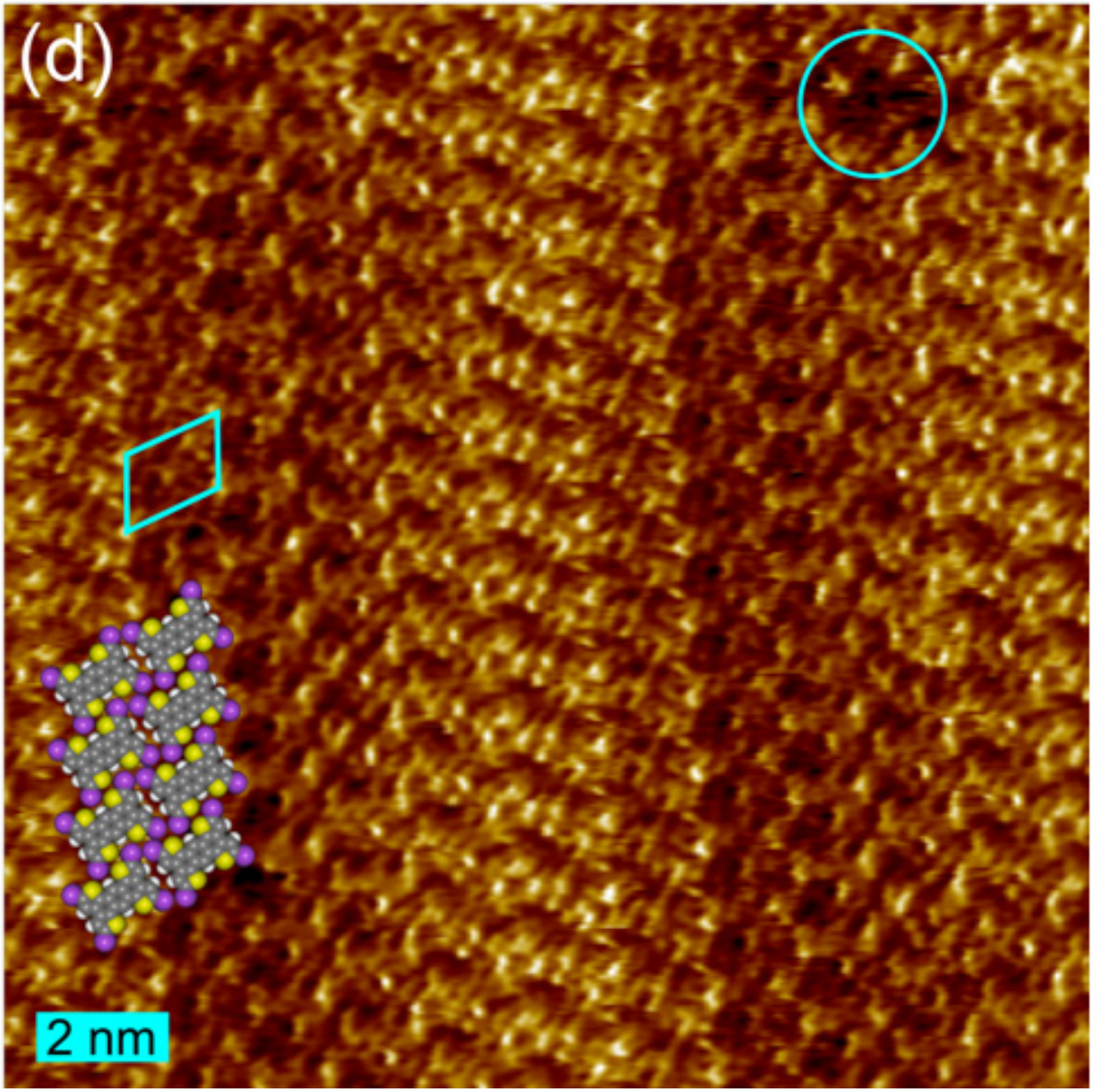

Figure S11. Larger-scale copies of the Fig. 1d.

IV. Bibliography

1 M. J. Frisch, G. W. Trucks, H. B. Schlegel, G. E. Scuseria, M. A. Robb, J. R. Cheeseman, G. Scalmani, V. Barone, B. Mennucci, G. A. Petersson, H. Nakatsuji, M. Caricato, X. Li, H. P. Hratchian, A. F. Izmaylov, J. Bloino, G. Zheng, J. L. Sonnenberg, M. Hada, M. Ehara, K. Toyota, R. Fukuda, J. Hasegawa, M. Ishida, T. Nakajima, Y. Honda, O. Kitao, H. Nakai, T. Vreven, J. A. M. Jr., J. E. Peralta, F. Ogliaro, M. Bearpark, J. J. Heyd, E. Brothers, K. N. Kudin, V. N. Staroverov, R. Kobayashi, J. Normand, K. Raghavachari, A. Rendell, J. C. Burant, S. S. Iyengar, J. Tomasi, M. Cossi, N. Rega, J. M. Millam, M. Klene, J. E. Knox, J. B. Cross, V. Bakken, C. Adamo, J. Jaramillo, R. Gomperts, R. E. Stratmann, O. Yazyev, A. J. Austin, R. Cammi, C. Pomelli, J. W. Ochterski, R. L. Martin, K. Morokuma, V. G. Zakrzewski, G. A. Voth, P. Salvador, J. J. Dannenberg, S. Dapprich, A. D. Daniels, Ö. Farkas, J. B. Foresman, J. V. Ortiz, J. Cioslowski, and D. J. Fox, *Gaussian 09, Revision A.02, Gaussian, Inc., Wallingford CT*, 2009.

2 Y. Zhao and D. Truhlar, *Theor. Chim. Acta*, 2008, 120, 215-241.

3 Y. Zhao and D. G. Truhlar, *Acc. Chem. Res.*, 2008, 41, 157-167.

4 S. F. Boys and F. Bernardi, *Molecular Physics: An International Journal at the Interface Between Chemistry and Physics*, 1970, 19, 553-566.

5 K. N. Kirschner, J. B. Sorensen, and J. P. Bowen, *Journal of Chemical Education*, 2007, 84.

6 E. D. Glendening, A. E. Reed, J. E. Carpenter, and F. Weinhold, *NBO Version 3.1*.